Earth Syst. Sci. Data Discuss., doi:10.5194/essd-2015-40, 2016
Manuscript under review for journal Earth Syst. Sci. Data
Published: 18 January 2016

A synthetic data set of high-spectral resolution infrared spectra for the Arctic atmosphere

C. J. Cox[1,2], P. M. Rowe[3,4], S. P. Neshyba[5], and V. P. Walden[6]

[1] {Cooperative Institute for Research in Environmental Sciences, University of Colorado, Boulder}

[2] {NOAA Earth System Research Laboratory, Physical Sciences Division, Boulder, CO}

[3] {Department of Geography, University of Idaho, Moscow, ID}

[4] {Departamento de Física, Universidad de Santiago de Chile, Santiago, Chile}

[5] {Department of Chemistry, University of Puget Sound, Tacoma, WA}

[6] {Department of Civil and Environmental Engineering, Washington State University, Pullman, WA}

Correspondence to: C. J. Cox (christopher.j.cox@noaa.gov)

Earth Syst. Sci. Data Discuss., doi:10.5194/essd-2015-40, 2016
Manuscript under review for journal Earth Syst. Sci. Data
Published: 18 January 2016

Abstract

Retrievals of cloud microphysical and macrophysical properties from ground-based and satellite-based infrared remote sensing instruments are critical for understanding clouds. However, retrieval uncertainties are difficult to quantify without a standard for comparison. This is particularly true over the polar regions where surface-based data for a cloud climatology are sparse, yet clouds represent a major source of uncertainty in weather and climate models. We describe a synthetic high-spectral resolution infrared data set that is designed to facilitate validation and development of cloud retrieval algorithms for surface- and satellite-based remote sensing instruments. Since the data set is calculated using pre-defined cloudy atmospheres, the properties of the cloud and atmospheric state are known *a priori*. The atmospheric state used for the simulations is drawn from radiosonde measurements made at the North Slope of Alaska (NSA) Atmospheric Radiation Measurement (ARM) site at Barrow, Alaska (71.325 °N, 156.615 °W), a location that is generally representative of the western Arctic. The cloud properties for each simulation are selected from statistical distributions derived from past field measurements. Upwelling (at 60 km) and downwelling (at the surface) infrared spectra are simulated for 222 cloudy cases from 50 - 3000 cm^{-1} (3.3 to 200 μm) at monochromatic (line-by-line) resolution at a spacing of ~0.01 cm^{-1} using the Line-by-line Radiative Transfer Model (LBLRTM) and the discrete-ordinate-method radiative transfer code (DISORT). These spectra are freely available for interested researchers from the ACADIS data repository (doi: 10.5065/D61J97TT).

Earth Syst. Sci. Data Discuss., doi:10.5194/essd-2015-40, 2016
Manuscript under review for journal Earth Syst. Sci. Data
Published: 18 January 2016

1 Introduction

Cloud properties, including height, temperature, particle size, and thermodynamic phase modulate precipitation development, cloud lifetime, and cloud radiative forcing. In climate change scenarios, models show that radiative forcing by Arctic clouds amplifies greenhouse warming, with the largest model errors in winter and spring when longwave warming dominates (Vavrus et al., 2009). Thus, an accurate understanding of the radiative effects of Arctic clouds, as well as quality estimates of observed cloud properties, are needed to advance research focused on the role of clouds in climate and to support modeling applications at many scales.

In the polar regions, progress toward this goal is hampered by limited data, large uncertainties, and systematic biases in different remote sensing approaches to retrieving cloud properties. Passive infrared sensors are well suited to examine the interplay between clouds and infrared radiation because they measure infrared radiation directly and can be used to retrieve cloud properties. Passive infrared sensors have been used to retrieve cloud properties from satellite platforms, providing broad spatial coverage (e.g., Wang and Key 2005; Strabala et al., 1994; Baum et al., 2000; Li et al., 2005; Kay and Gettelman, 2009; Kahn et al, 2014), as well as from surface observatories, providing high temporal resolution (e.g. Rathke et al., 2002a,b; Turner et al. 2003; Turner, 2005; Zhao et al., 2012; Garrett and Zhao, 2013; Cox et al., 2014). But because retrieval algorithms based on these sensors include radiative-equivalent assumptions particular to the infrared part of the spectrum, the retrieved cloud properties do not always agree with results obtained from other types of sensors: they are most sensitive to optically thin clouds near the instrument (i.e. high clouds for satellite-based sensors and low clouds for surface-based sensors), typically are layer-averaged through all cloud columns, and generally are more sensitive to liquid than ice, primarily due to how differences in the geometries of ice and liquid hydrometeors affect their infrared radiance (e.g., Garrett and Zhao, 2006). Numerous inter-comparison studies report systematic differences between cloud properties retrieved from infrared sensors and results from other sensors (e.g., Shupe et al., 2008; Dong et al., 2008; Karlsson and Dybbroe, 2010; Liu et al., 2010; Minnis et al., 2011; Vogelmann et al., 2012; Zhao et al., 2012; Chan and Comiso, 2013; Jin and Nasiri, 2014).

Biases are difficult to reconcile when working with real data alone. In large part, this is due to fundamental differences in perspective and measurement sensitivity between different sensor

Earth Syst. Sci. Data Discuss., doi:10.5194/essd-2015-40, 2016
Manuscript under review for journal Earth Syst. Sci. Data
Published: 18 January 2016

types: some instruments record cloud properties on a time scale that is fast compared to the time scale of cloud evolution, for example, while others yield average properties. A similar situation arises due to variations in field of view. Even within the set of infrared remote sensing algorithms currently in use, comparative evaluation of different algorithms is often not possible because the actual cloud properties are not known.

Thus, alternative evaluation approaches (e.g., Pincus et al., 2012) are needed to better constrain biases, facilitate algorithm development, and advance interpretation of results. Simulated data sets, though idealized, reduce the number of sources of uncertainty, thereby permitting a more detailed evaluation of many aspects of individual methodologies and measurement sensitivities. In a simulated data set, the properties of interest are known *a priori* and the assumptions associated with the data set are controlled.

In this manuscript, we describe a simulated data set that can be used to represent a cloud climatology for the Arctic as viewed from the surface or space by passive infrared sensors. The data set is applicable to studies focusing on assessing uncertainties in cloud properties derived from hyperspectral and narrow-band infrared radiances, which currently represent a substantial source of data for the Arctic. The inclusion of a wide range of cloud properties is useful for such studies, as well as making the dataset useful for studies focused on the infrared radiative effects of Arctic clouds. The data set described here is based on atmospheric profiles measured by radiosoundings from Barrow, Alaska (71.325 °N, 156.615 °W, 8 m), a location thought to be generally representative of the far-western Arctic atmosphere (Dong and Mace, 2003; Dong et al., 2010; Shupe et al., 2011; Cox et al., 2012). Because the data set is intended to be representative of the Arctic in general, it is only loosely based on Barrow; the main objective is to encompass the range of properties expected in the Arctic. Cloud properties are generalized from results reported for the western Arctic and Canadian Archipelago regions (Shupe et al., 2011; Shupe, 2011; Cox et al., 2014). The data set consists of infrared radiative transfer calculations of 222 unique "cloudy sky" cases based on varying cloud properties for 30 unique atmospheric states (e.g. temperature, humidity, and CO_2 profiles) that are representative of scenes containing clouds. The spectral range is 50 to 3000 cm^{-1} (200 – 3.3 μm) at monochromatic, or line-by-line resolution, spaced at ~ 0.01 cm^{-1}. Through convolution of the simulated spectra with an

Earth Syst. Sci. Data Discuss., doi:10.5194/essd-2015-40, 2016
Manuscript under review for journal Earth Syst. Sci. Data
Published: 18 January 2016

instrument response function (e.g., Beer 1992), the data set can be customized to mimic data acquired by a range of instrumentation. The data set is available for community use; data access information is provided in Section 6.

2 Radiative Transfer Models

To simulate upwelling and downwelling infrared spectra, two radiative transfer models are used. The Line-By-Line Radiative Transfer Model (LBLRTM), version 12.2, (Clough et al., 1992; Clough et al., 2005) is used initially to calculate vertical profiles of infrared optical depths of radiatively-active gases under clear-sky conditions. LBLRTM has been validated extensively (e.g., Clough et al. 1992; Clough et al., 2005; Delamere, 2010; Alvarado et al., 2013).

LBLRTM requires vertical profiles of temperature and radiatively-active gases (e.g. water vapor, carbon dioxide, and ozone) as input to simulate clear-sky optical depth profiles and radiance. Preparation of the profiles is described in Section 3.1. The LBLRTM calculations were performed line-by-line from 50 to 3000 cm^{-1} (3.3 - 200 μm) using the 2008 version of the high-resolution transmission molecular absorption database (HITRAN) (Rothman et al., 2009). The gaseous optical depth profiles are then used together with cloud properties as input to a program for calculating discrete-ordinate-method radiative transfer in scattering and emitting layered media (DISORT) (Stamnes et al., 1988) to simulate cloudy-sky spectra. For this data set, only single-layered clouds were calculated. Both DISORT and LBLRTM simulate radiation in a plane-parallel model atmosphere.

DISORT performs radiative transfer at a given wavenumber and requires a variety of input parameters. (Even though DISORT is monochromatic, a small wavenumber interval is specified for calculation of the Planck radiation.) A Matlab code ("runDisort.m" available at https://github.com/prowe12/runDisort) was developed for organizing the inputs, running DISORT at each wavenumber to calculate the infrared radiance at the surface or top of atmosphere, and combining the radiances into a high-resolution spectrum. Inputs to runDisort.m include wavenumber, gaseous optical depths (e.g., from LBLRTM), and the temperature profile, as well as the cloud properties (cloud layer, visible optical depths, and effective radii for liquid and ice). Additional inputs are as follows. For downwelling spectra, the viewing angle is set to 0°

Earth Syst. Sci. Data Discuss., doi:10.5194/essd-2015-40, 2016
Manuscript under review for journal Earth Syst. Sci. Data
Published: 18 January 2016

relative to zenith, while for upwelling the viewing angle is 180°. The solar zenith angle is calculated for a particular date and location, where the chosen dates represent all four seasons (see Section 3.1) and the location was chosen in the Canadian Arctic at ~80°N, 86°W. Thus, solar angles are typically low (note that for wavenumbers smaller than about 2000 cm^{-1}, the influence of solar radiation is small). The surface type is set to Lambertian, and the surface albedo is determined from the surface emissivity measurements for ice/snow from the Moderate Resolution Imaging Spectrometer (MODIS) University of California, Santa Barbara (UCSB) emissivity library. Beyond the wavenumber range of the emissivity library (687-998 cm^{-1}), the emissivity is assumed to be spectrally flat and equivalent to the values at the boundaries. The Kurucz solar source function is used (Kurucz et al., 1992) to determine the solar input.

The single-scattering albedo, asymmetry parameter, phase function moments, and extinction, absorption, and scattering efficiencies were calculated from Mie theory assuming spheres for both liquid and ice (Wiscombe, 1979, 1980). (Spheres were specifically used for ice to simplify the dataset and any associated retrievals.) Mie calculations require the complex indices of refraction of the cloud particles as well as specification of the particle radius. Subsequently, the single scattering properties were averaged for a log-normal distribution of particle sizes with geometric mean radius,

$$r_g = \frac{r_e}{e^{2.5 \ln(\sigma_g)}}, \tag{1}$$

where r_e specifies effective radius, as described by Neshyba et al. (2003); note that here σ_g was chosen to be 0.331.

In model layers containing the cloud, runDisort.m adds the wavenumber-dependent infrared cloud optical depth (τ) to the gaseous optical depth. The cloud optical depth is determined from the visible optical depth (τ_{vis}) independently for each phase. For example, for liquid

$$\tau_{liq} = \frac{\tau_{vis,liq}}{2} Q_{ext,liq}(r_{liq}), \tag{2}$$

where $Q_{ext,liq}$ is the extinction cross section. [For ice, replace *liq* with *ice* in Eq. (2).] This work uses new temperature-dependent indices of refraction for liquid water at 240, 253, 263, 273 and 300 K (see Rowe et al., 2013 and references therein). To estimate the liquid optical depth of the cloud, optical depths are computed at two temperatures, one falling just below the mean cloud

Earth Syst. Sci. Data Discuss., doi:10.5194/essd-2015-40, 2016
Manuscript under review for journal Earth Syst. Sci. Data
Published: 18 January 2016

temperature and the other just above it, and then a weighted mean is taken. For ice, temperature dependencies are not included. Mixed phase clouds are modeled as external mixture: the sum of liquid and ice optical depths is used.

3 Specification of the atmospheric state

The initial step in simulating infrared spectra is to specify the properties of the atmosphere. In the infrared, the relevant parameters are the vertical profiles of temperature and concentrations of gases that absorb and emit significantly in the spectral region of interest. First, a representative set of vertical profiles of temperature and concentration of atmospheric gases is selected (Section 3.1). Second, a realistic description of the macrophysical properties of clouds (i.e., height and physical thickness) is determined for each profile (Section 3.2). Finally, for each cloud, a range of microphysical properties (i.e., particle size, phase) and optical properties (i.e., optical depth) is defined (Section 3.3). Each spectrum represents a radiative transfer calculation of one of the profiles containing a cloud with a set of properties that satisfy the criteria of the study.

3.1 Preparation of atmospheric profiles

It is important that the profiles of temperature and humidity be realistic, and that the vertical position and extent of clouds also be realistic for individual profiles. Therefore, a small, representative sample of temperature and humidity profiles from radiosondes, which may include features such as cloud-top inversions, was used instead of a climatological mean, which averages out such features. An initial set of 796 radiosondes launched in 2012 by the U.S. Department of Energy (DOE) Atmospheric Radiation Measurement (ARM) program at the North Slope of Alaska (NSA) site (Stamnes et al., 1999) was examined. ARM NSA launched Vaisala RS-92 radiosondes, typically at 0600 and 1800 UTC, but sometimes at other times during the day. Possibly spurious temperature inversions within the lowest 100 m were removed by linearly interpolating to the surface. For reference, the radiosondes from Barrow in 2012 were similar to the radiosonde profiles from over the Arctic Ocean north of Barrow acquired during the Surface Heat Budget of the Arctic Ocean (SHEBA) (Uttal et al., 2002) drifting observatory in 1997 and 1998, but were slightly warmer and moister with slightly stronger temperature inversions. Radiosondes were only deemed valid for selection if they reached at least 10 km, reducing the set

Earth Syst. Sci. Data Discuss., doi:10.5194/essd-2015-40, 2016
Manuscript under review for journal Earth Syst. Sci. Data
Published: 18 January 2016

from 796 to 784. The profiles were linearly interpolated to a common grid of 41 vertical levels that are described in detail later in this section. References to the ARM-archived files containing the original radiosonde data are included with the dataset.

The data set focuses on atmospheric profiles containing clouds. Because clear and cloudy-sky profiles may differ, only profiles likely to represent cloudy times were selected. These were identified by the presence of one or more layers where the relative humidity with respect to water was greater than 95% between the surface and 8 km, where Arctic clouds are typically found (Shupe et al., 2011). (Throughout this manuscript, "relative humidity" is defined as being with respect to water.) This threshold (rather than requiring 100% relative humidity) was chosen because humidity sensors are typically biased low in the dry polar atmosphere (Miloshevich et al., 2006; and Vömel et al., 2007; Rowe, et al., 2008); relative humidities at model cloud heights were subsequently set to 100%, as described below. Of the remaining 784 radiosondes, 522 (67%) are good candidates for containing clouds. Since the number of calculations that can be performed is limited because of the long computational time, a random selection of 30 of the 522 (6%) "cloudy" profiles is used for the final data set.

Figure 1 shows how the thirty selected profiles are distributed in time throughout the year. The selected profiles exclude some of the lowest surface temperatures because those conditions most likely represent clear-skies. All seasons are represented, but more radiosondes are from summer and autumn than winter and spring, which is consistent with the fact that the cloud fraction is higher in summer and autumn (80-95% of time) than in winter and spring (60-80%) at Barrow (Shupe et al., 2011). The temperature and humidity profiles for these selections are similar in mean and variance to the full 2012 Barrow data set, as shown in Figures 2a and 2b. The model atmosphere is divided into 40 layers extending from the surface to 60 km (atmospheric pressure at 60 km is less than 1 mb). Since levels in the stratosphere are relatively coarse, levels between 28 km and 33 km are qualitatively set to fully capture the profile of ozone. Temperature, humidity, and trace gas concentrations are specified at 41 layer boundaries, spaced by 0.1 km from 0 to 1 km, by 0.2 km from 1 to 2 km, and then at 2.4, 2.8, 3.2, 4, 5, 6, 7, 8, 9, 10, 11, 12, 14, 17, 20, 25, 28, 33, 36.4, 39.6, 43, 46, 50, 56, and 60 km. DISORT models the change in temperature across a layer by assuming the Planck function changes linearly with optical depth; this approximation leads to a requirement that the temperature differential across a layer be < 10

Earth Syst. Sci. Data Discuss., doi:10.5194/essd-2015-40, 2016
Manuscript under review for journal Earth Syst. Sci. Data
Published: 18 January 2016

Open Access Earth System Science Data Discussions

K (Stamnes et al, 2000). Thus to avoid errors due to large temperature variations across the layers, the boundaries are chosen such that temperature variations are < 7 K below 3 km, where most clouds are positioned (see Section 3.2 for a discussion of cloud height) and < 10 K for all layers, as shown in Figure 3.

For computational efficiency, we truncate the model atmosphere at the height above which layer optical depths begin to fall below 10^{-5}. For the atmospheric layering chosen, at highly transparent wavenumbers, the optical depth can fall below 10^{-5} in the upper troposphere, while at other wavenumbers, layer optical depths may be > 10^{-5} up to 60 km. Thus, at each wavenumber, the profiles used in the DISORT calculation terminate at 60 km or the height at which the layer optical depth falls to 10^{-5}, whichever is lower. Radiance differences due to truncating the atmosphere when the optical depth falls below 10^{-5} are found to be quite small (sensitivity studies indicate that errors due to omitting these layers are on the order of 10^{-4} mW (m^2 sr cm^{-1})$^{-1}$).

Humidity and temperature profiles above 18 km use the subarctic summer and subarctic winter standard atmospheres (McClatchey et al., 1972); all selected radiosoundings terminated above this height. Ozone, nitrous oxide, carbon monoxide, methane, and oxygen are also set using standard atmospheres (McClatchey et al., 1972). The subarctic winter model is used for the months of November through February, the subarctic summer is used for June through August, and the mean is used for the other months. Carbon dioxide concentrations are from monthly mean surface flask measurements from Barrow acquired in 2010 by the NOAA Earth System Research Laboratory (ESRL) Global Monitoring Division (GMD) (Conway et al., 2011); a constant mixing ratio with height is assumed.

3.2 Cloud macrophysical properties

Cloud macrophysical properties (cloud base and top heights) are set qualitatively by analysis of each of the 30 individual atmospheric profiles. Cloud base and top heights determine the physical thickness. The thermodynamic temperature structure of each cloud is that of the model layer(s) in which it was placed. As described in the previous section, at least one layer in each profile had a relative humidity greater than 95%. This moist layer could sometimes span multiple model atmospheric layers, particularly in the lower atmosphere where many model layers are physically thin, but where Arctic clouds are likely to be physically thick. When only a single layer boundary

Earth Syst. Sci. Data Discuss., doi:10.5194/essd-2015-40, 2016
Manuscript under review for journal Earth Syst. Sci. Data
Published: 18 January 2016

is moist, the adjacent layer (either above or below) with the highest humidity is identified as a cloud boundary. Some layers with relative humidity less than 95% that are adjacent to moist layer boundaries are identified as containing a cloud because other identifying characteristics were present, such as a cloud-top inversion. In all "cloudy" layers, the relative humidity is set to 100%. Seven of the 30 profiles can be considered cloudy at two non-successive layers in the atmospheric column. These profiles are used twice, once for the lower cloud and once for the upper cloud, but two clouds are never defined at the same time in keeping with the criteria of modeling single clouds only. Therefore, a total of 37 clouds were identified using the 30 profiles. Figure 4 shows an example of a profile; the cloud location is indicated in gray.

A summary of the cloud macrophysics is shown in Figure 5. The distribution of cloud base heights (Figure 5a) is similar to that reported for Barrow and SHEBA in Shupe et al. (2011), but the cloud top heights (Figure 5a) and thus also the cloud thicknesses (Figure 5b), are somewhat lower than those reported by Shupe et al. (2011). Distributions of cloud layer-mean thermodynamic temperature (Figure 5c) are also reasonable when compared to the distributions reported for Barrow and SHEBA by Shupe et al. (2011). Figure 6 shows the relationship between cloud base height and other macrophysical properties. Mean cloud temperatures (Figure 6a) generally decrease with increasing height, as is generally true in the atmosphere, with a weaker correlation in the lowest 1 km, likely due to the near-surface temperature inversion, which is common in the Arctic. Because model layers were defined to get thicker going up in the atmosphere, the highest clouds are unrealistically physically thick (Figure 6b), and therefore the temperature gradient through the layer (Figure 6c), is also less realistic. However, this layering was chosen for simplicity, consistency, and computational efficiency.

3.3 Cloud microphysical and optical properties

This section describes the parameterization of cloud microphysical and optical properties, including optical depth, particle size (effective radius), thermodynamic phase (ice fraction), ice water path (IWP), and liquid water path (LWP). For each simulation, visible optical depth, ice fraction, effective radius of liquid (if present) and effective radius of ice (if present) are randomly

Earth Syst. Sci. Data Discuss., doi:10.5194/essd-2015-40, 2016
Manuscript under review for journal Earth Syst. Sci. Data
Published: 18 January 2016

selected from pre-determined distributions for the simulations; IWP and LWP are calculated based on these selections.

Figure 7 shows the distributions of each of the parameterized microphysical and optical properties for the 222 simulations. The distributions of effective radii are modeled as gamma distributions to be similar to distributions retrieved from ground-based infrared spectral observations at SHEBA (Turner, 2005) and Eureka, Canada (80.053 °N, 86.417 °W, 10 m) (Cox et al., 2014). The means were set to 10 µm for liquid and 25 µm for ice, which are reasonable estimates for Arctic particle sizes (Turner, 2005). Following the results from Cox et al. (2014) and Turner (2005), the distribution shape parameter is set subjectively to $\alpha = 5$ for liquid and $\alpha = 0$ for ice. An additional consideration in setting the shape parameter is to ensure that the distributions overlap, as they do in the real atmosphere, to make sure that retrieval algorithms tested using this data set do not rely on particle size to determine phase. The overlap is approximately 1/3 of the area under each distribution.

Cloud visible optical depths are selected randomly from a uniform distribution of transmission ($\mathfrak{I}$) between 0 and 0.98; the visible optical depth is then $-\ln[\mathfrak{I}]$. The maximum transmission is set to 0.98 because this is approximately equivalent to an optical depth of 0.02; such a small optical depth is typically below the threshold for detecting a cloud for most currently used instruments and was chosen purposefully so the dataset is useful for testing the limits of retrieval capability. Similarly, the upper optical depth threshold is above the typical threshold for sensitivity to cloud microphysical properties in the infrared (optical depth of ~6), allowing for testing retrieval limitations. The resulting distribution, shown in Figure 7b, is quasi-logarithmic, as are distributions of optical depth retrieved from infrared observations in the Arctic (Turner, 2005; Cox et al., 2014). This method for building an optical depth distribution is practical because it results in many thin clouds, but not as many as an exponential distribution, and only a few clouds with optical depths greater than 6-7, above which clouds are nearly optically opaque.

Phase partitioning is set so that the probability of liquid-only and ice-only clouds is each 1:6, and the probability of a mixed-phase cloud is 2:3. The actual proportions of the final data set are shown in Figure 7c. These proportions are not meant to reflect a climatological distribution representative of the Arctic, but rather to ensure that a sufficient number of each phase is

Earth Syst. Sci. Data Discuss., doi:10.5194/essd-2015-40, 2016
Manuscript under review for journal Earth Syst. Sci. Data
Published: 18 January 2016

represented especially for mixed-phase clouds, which are common in the Arctic (Turner, 2005; Shupe et al., 2008; de Boer et al., 2009; Shupe, 2011; Cox et al., 2014). Ice fractions for mixed-phase clouds are drawn from a uniform distribution between 0.01 and 0.99. The distribution of ice fraction in mixed-phase clouds in the final data set is shown in Figure 7d.

4 Modelled infrared spectra

Figures 8a and b show examples of simulated line-by-line spectra (the spectral grid is ~2.55×10^{-4} cm^{-1} for LBLRTM and ~0.01 cm^{-1} for DISORT) in three spectral ranges (or channels). For each atmospheric profile, clear-sky radiances were created using LBLRTM and are provided together with the cloudy-sky profiles (upwelling clear-sky radiances created with LBLRTM use the same surface emissivity/reflectivity characteristics as cloudy-sky radiances created with DISORT). An overlap of 50 cm^{-1} at the edges of the channels ensures that errors incurred near the edges are negligible when combining the channels. The clear-sky radiance is also shown for reference. The effect of the cloud is to increase the baseline of the spectrum, which is close to zero in the atmospheric window (800 to 1300 cm^{-1}), for the clear-sky case. For the cloud shown, the cloud is thin enough that strong gaseous emission lines are clearly evident.

The simulations can be convolved with an instrument response function to produce a simulation that matches the output from an actual instrument (e.g., Beer, 1992). For example, Figures 9a and 9b show a downwelling spectrum from the perspective of the surface at a variety of different resolutions (0.1, 0.5, 1, 2, and 4 cm^{-1}), where the spectra were created by convolving the line-by-line spectra with the sinc function (or, in practice, by multiplying the corresponding interferograms by boxcar functions and taking the Fourier transform). Figures 9c and 9d show the same for upward directed radiances from the perspective of the top of the atmosphere (TOA, defined here as 60 km), representing radiances that would be measured from satellites.

Spectra at a variety of instrument resolutions can be used to test cloud height retrievals and microphysical property retrievals, as well as to test methods for running DISORT using gaseous optical depths that have been modified to account for instrument resolution. For uses such as these, the sources of retrieval errors can be tested as follows. Random noise can be simulated and added to the simulated radiances. To simulate errors in the atmospheric state, retrievals can be

Earth Syst. Sci. Data Discuss., doi:10.5194/essd-2015-40, 2016
Manuscript under review for journal Earth Syst. Sci. Data
Published: 18 January 2016

performed using atmospheric profiles that have been perturbed. Because the dataset consists of so many cases, errors can be drawn from a random distribution characterized by the desired mean and standard deviation so that errors vary from case to case. Because the data are simulated, these sources of error, as well as model errors, can be quantified.

5 Conclusions

A synthetic, monochromatic (line-by-line) resolution data set of spectral infrared radiances is described that is based on the atmospheric state and cloud conditions typical of the western Arctic. The data set includes radiative transfer calculations from the perspective of the surface and the top of the atmosphere (60 km) and is thus applicable to researchers working with surface- or satellite-based measurements. The data set is designed to provide an idealized framework for the development and testing of cloud-property retrieval algorithms in which the assumptions are controlled and the properties of the clouds are known *a priori*. This addresses an important knowledge gap demonstrated by the results of numerous studies reporting systematic, but only weakly traceable differences in intercomparisons between measurement and retrieval methodologies (e.g., Shupe et al., 2008; Dong et al., 2008; Liu et al., 2010; Minnis et al., 2011; Vogelmann et al., 2012; Zhao et al., 2012; Chan and Comiso, 2013). The data set may also be useful for other applications as well, such as research on cloud-surface radiative interactions, trace gas retrievals, or investigations of the effect of instrument resolution.

6 Data accessibility

Upwelling (at 60 km) and downwelling (at the surface) simulated clear-sky and all-sky infrared spectra, cloud properties, and atmospheric state profiles of temperature, pressure, and radiatively-active gases are available in the Network Common Data Format (netCDF) (e.g., http://www.unidata.ucar.edu/software/netcdf/). The data set contains 222 unique cases from 50 - 3000 cm^{-1} (3.3 to 200 µm) at a spectral resolution of ~0.01 cm^{-1} (all-sky) and line-by-line resolution (clear-sky). The spectral range is distributed across three channels (100-510 cm^{-1}, 460-2055 cm^{-1}, and 2005-3000 cm^{-1}), each in separate files. Interested researchers may download the data from ACADIS (http://www.aoncadis.org) and are encouraged to cite the use of the data using the associated digital object identifier (doi: 10.5065/D61J97TT).

Author contributions

C. J. Cox, V. P. Walden, and P. M. Rowe conceived and designed the data set and performed the simulations. P. M. Rowe and S. P. Neshyba developed computer code used for the simulations. C. J. Cox prepared the manuscript with contributions from all co-authors.

Acknowledgements

This work was supported by the National Science Foundation's Arctic Observing Network (AON) (NSF ARC-1108451). Cox also received support from the NOAA Climate Program Office (CPO) Arctic Research Program (ARP) and the Cooperative Institute for Research in Environmental Sciences (CIRES) Visiting Fellows Program. Rowe received support from NSF award ARC-1108451 and from USACH-DICYT 041331CC_DAS and FONDECYT 1151034. Neshyba was supported by NSF award CHE-1306366 for this work NOAA Earth System Research Laboratory (ESRL) Global Monitoring Division (GMD) archive of CO_2 measurements is available from ftp://aftp.cmdl.noaa.gov/data/trace_gases/co2/flask/surface/. The U.S. Dept. of Energy (DOE) Atmospheric Radiation Measurement (ARM) program data are available from the ARM archive, http://www.arm.gov. Moderate Resolution Imaging Spectrometer (MODIS) University of California, Santa Barbara (UCSB) emissivity library is available from http://www.icess.ucsb.edu/modis/EMIS/html/em.html. We acknowledge the ACADIS data portal, where the data is archived for community use: http://www.aoncadis.org.

References

Alvarado, M.J., Payne, V.H., Mlawer, E.J., Uymin, G., Shephard, M.W., Cady-Pereira, K.E., Delamere, J., and Moncet, J.L.: Performance of the line-by-line radiative transfer model (LBLRTM) for temperature, water vapor, and trace gas retrievals: Recent updates evaluated with IASI case studies, Atmos. Chem. Phys., 13, doi:10.5194/acp-2012-813, 2013.

Earth Syst. Sci. Data Discuss., doi:10.5194/essd-2015-40, 2016
Manuscript under review for journal Earth Syst. Sci. Data
Published: 18 January 2016

Baum, B.A., Kratz, D.P., Yang, P., Ou, S.C., Hu, Y., Soulen, P.F., Tsay, S.-C.L.: Remote sensing of cloud properties using MODIS airborne simulator imagery during SUCCESS 1. Data and models. J. Geophys. Res., 105 (D9), 11767-11780, doi: 10.1029/1999JD901089, 2000.

Beer, R.: Remote sensing by Fourier transform spectrometry, Wiley-Interscience, New York, 1992.

Chan, M.A., and Comiso, J.C.: Arctic cloud characteristics as derived from MODIS, CALIPSO, and CloudSat, J. Climate, 26, 3285-3306, doi:10.1175/JCLI-D-12-00204.1, 2013.

Clough, S.A., Shephard, M.W., Mlawer, E.J., Delamere, J.S., Iacono, M.J., Cady-Pereira, K., Boukabara, S., and Brown, P.D.: Atmospheric radiative transfer modeling: a summary of the AER codes, Short Communication, J. Quant. Spectrosc. Ra., 91, 233-244, doi:10.1016/j.jqsrt.2004.05.058, 2005.

Clough, S. A., Iacono, J.M., and Moncet, J.-L.: Line-by-line calculations of atmospheric fluxes and cooling rates: Application to water vapor, J. Geophys. Res-Atmos., 97(D14), 15,761–15,785, doi:10.1029/92JD01419, 1992.

Conway, T.J., Lang, P.M., and Masarie, K.A.: Atmospheric carbon dioxide dry air mole fractions from the NOAA ESRL Carbon Cycle Cooperative Global Air Sampling Network, 1968–2010, 2011. [Available online at ftp://aftp.cmdl.noaa.gov/data/trace_gases/co2/flask/surface/].

Cox, C.J., Walden, V.P., and Rowe, P.M.: A comparison of atmospheric conditions at Eureka, Canada, and Barrow, Alaska (2006-2008), J. Geophys. Res-Atmos., 117, D12204, doi:10.1029/2011JD017164, 2012.

Cox, C.J., Turner, D.D., Rowe, P.M., Shupe, M.D., and Walden, V.P.: Cloud microphysical properties retrieved from downwelling infrared radiance measurements made at Eureka, Nunavut, Canada (2006-09), J. Appl. Meteorol. Clim., 53, 772-791, doi:10.1175/JAMC-D-13-0113.1, 2014.

de Boer, G., Eloranta, E.W., and Shupe, M.D.: Arctic mixed-phase stratiform cloud properties from multiple years of surface-based measurements at two high-latitude locations, J. Atmos. Sci., 66, 2874-2887, doi: 10.1175/2009JAS3029.1, 2009.

Earth Syst. Sci. Data Discuss., doi:10.5194/essd-2015-40, 2016
Manuscript under review for journal Earth Syst. Sci. Data
Published: 18 January 2016

Delamere, J.S., Clough, S.A., Payne, V.H., Mlawer, E.J., Turner, D.D., and Gamache, R.R.: A far-infrared radiative closure study in the Arctic: Application to water vapor, J. Geophys. Res-Atmos., 115, D17106, doi:10.1029/2009JD012968, 2010.

Dong, X. and Mace, G.G.: Arctic stratus cloud properties and radiative forcing derived from ground-based data collected at Barrow, Alaska, J. Climate, 16, 445-461, doi:10.1175.1520-0442(2003)016>0445:ASCPAR>2.0.CO;2, 2003.

Dong, X., Minnis, P., Xi, B., Sun-Mack, S., and Chen, Y.: Comparison of CERES-MODIS stratus cloud properties with ground-based measurements at the DOE ARM Southern Great Plains site, J. Geophys. Res-Atmos., 113, D03204, doi:10.1029/2007JD008438, 2008.

Dong, X., Xi, B., Crosby, K., Long, C.N., Stone, R.S., and Shupe, M.D.: A 10 year climatology of Arctic cloud fraction and radiative forcing at Barrow, Alaska, J. Geophys. Res-Atmos., 115, D17212, doi:10.1029/JD013489, 2010.

Garrett, T.J. and Zhao, C.: Increased Arctic cloud longwave emissivity associated with pollution from mid-latitudes, Nature, 440, 787-789, doi:10.1038/nature04636, 2006.

Garrett, T.J. and Zhao, C.: Ground-based remote sensing of thin clouds in the Arctic, Atmos. Meas. Tech., 6, 1227-1243, doi:10.5194/amt-6-1227-2013, 2013.

Jin, H. and Nasiri, S.L.: Evaluation of AIRS cloud-thermodynamic-phase determination with CALIPSO. J. Appl. Meteor. Climatol., 53, 1012-1027, doi: 10.1175/JAMC-D-13-0137.1, 2014.

Kahn, B.H., Irion, F.W., Dang, V.T., Manning, E.M., Nasiri, S.L., Naud, C.M., Blaisdell, J.M., Schreier, M.M., Yue, Q., Bowman, K.W., Fetzer, E.J., Hulley, G.C., Liou, K.N., Lubin, D., Ou, S.C., Susskind, J., Takano, Y., Tian, B., and Worden, J.R.: The Atmospheric Infrared Sounder version 6 cloud products, Atmos. Chem. Phys., 14, 399-426, doi:10.5194/acp-14-399-2014, 2014.

Karlsson, K. G., and Dybbroe, A.: Evaluation of Arctic cloud products from the EUMETSAT Climate Monitoring Satellite Application Facility based on CALIPSO-CALIOP observations, Atmos. Chem. Phys., 10(4), 1789-1807, doi: 10.5194/acp-10-1789-2010, 2010.

Earth Syst. Sci. Data Discuss., doi:10.5194/essd-2015-40, 2016
Manuscript under review for journal Earth Syst. Sci. Data
Published: 18 January 2016

Kay, J.E. and Gettelman, A.: Cloud influence on and response to seasonal Arctic sea ice loss, J. Geophys. Res-Atmos., 114, D18204, doi:10.1029/2009JD011773, 2009.

Kurucz, R.L.: Synthetic infrared spectra, in Infrared Solar Physics, IAU Symp. 154, edited by D.M. Rabin and J.T. Jefferies, Kluwer, Acad., Norwell, MA, 1992.

Li, J., Huang, H.-L., Liu, C.-Y., Yang, P., Schmit, T.J., Wei, H., Weisz, E., Guan, L., and Menzel, W.P.: Retrieval of cloud microphysical properties from MODIS and AIRS, J. Appl. Meteorol., 44, 1526-1543, doi: 10.1175/JAM2281.1, 2005.

Liu, Y., Ackerman, S.A., Maddux, B.C., Key, J.R., Frey, R.A.: Errors in cloud detection over the Arctic using a satellite imager and implications for observing feedback mechanisms, J. Climate, 23, 1894-1907, doi:10.1175/2009, 2010.

McClatchey, R.A., Fenn, R.W., Selby, J.E.A., Volz, F.E., and Garing, J.S.: Optical properties of the atmosphere, 3rd ed., Tech. Rep. AFCRL- 72–0497, 108 pp., Air Force Geophys. Lab., Hanscom AFB, Mass., 1972.

Miloshevich, L.M., Vömel, H., Whiteman, D.N., Lesht, B.M., Schmidlin, F.J., and Russo, F.: Absolute accuracy of water vapor measurements from six operational radiosonde types launched during AWEX-G and implications for AIRS validation, J. Geophys. Res-Atmos., 111, D09S10, doi:10.1029/2005JD006083, 2006.

Minnis, P., Sun-Mack, S., Chen, Y., Khaiyer, M.M., Yuhong, Y., Ayers, K., Brown, R.R., Dong, X., Gibson, S.C., Heck, P.W., Lin, B., Nordeen, M.L., Nguyen, L., Palikonda, R., Smith Jr., W.L., Spangenberg, S.A., Trepte, Q.Z., and Xi, B.: CERES Edition-2 cloud property retrievals using TRMM VIRS and Terra and Aqua MODIS data – Part II: Examples of average results and comparisons of with other data, IEEE T. Geosci. Remote, 49(11), 4401-4430, doi:10.1109/TGRS/2011.2144602, 2011.

Neshyba, S.P., Grenfell, T.C., and Warren, S.G.: Representation of a non-spherical ice particle by a collection of independent spheres for scattering and absorption of radiation: 2. Hexagonal columns and plates, J. Geophys. Res., 108(D15), 4448, doi:10.1029.2002JD003302, 2003.

Pincus, R., Platnick, S., Ackerman, S.A., Hemler, R.S., and Hoffman, R.J.P.: Reconciling simulated and observed views of clouds: MODIS, ISCCP, and the limits of instrument simulators, J. Climate, 25, 4699-4720, doi:10.1175/JCLI-D-11-00267.1., 2012.

Rathke, C., Fischer, J., Neshyba, S., and Shupe, M.: Improving IR cloud phase determination with 20 microns spectral observations, Geophys. Res. Lett., 29(8), 50–1–50–4. doi:10.1029/2001GL014594, 2002.

Rathke, C., Neshyba, S., Shupe, M., Rowe, P., and Rivers, A.: Radiative and microphysical properties of Arctic stratus clouds from multiangle downwelling infrared radiances. J. Geophys. Res., 107(D23), AAC 12–1–AAC 12–13. doi:10.1029/2001JD001545, 2002.

Rothman, L.S., Gordon, I.E., Barbe, A., Benner, D.C., Bernath, P.F., Birk, M., Boudon, V., Brown, L.R., Campargue, A., Champiom, J.-P., Chance, K., Coudert, L.H., Dana, V., Devi, V.M., Fally, S., Flaud, J.-M., Gamache, R.R., Goldman, A., Jacquemart, D., Kleiner, I., Lacome, N., Lafferty, W.J., Mandin, J.-Y., Massie, S.T., Mikhailenko, S.N., Miller, C.E., Moazzen-Ahmadi, N., Maumenko, O.V., Nikitin, A.V., Orphal, J., Perevalov, V.I., Perrin, A., Predoi-Cross, A., Rinsland, C.P., Rotger, M., Šimečková, Smith, M.A.H., Sung, K., and Tashkun, S.A.: The HITRAN 2008 molecular spectroscopic database, J. Quant. Spectrosc. Ra., 110(9-10), 533-572, doi:10.1016/j.jqrst.2009.02.013, 2009.

Rowe, P.M., Miloshevich, L.M., Turner, D.S., and Walden, V.: Dry Bias in Vaisala RS90 radiosonde humidity profiles over Antarctica, J. Atmos. Ocean. Tech., 25(9), 1529–1541. doi:10.1175/2008JTECHA1009.1, 2008.

Rowe, P.M., Neshyba, S., and Walden, V.P.: Radiative consequences of low-temperature infrared refractive indices for supercooled water clouds, Atmos. Chem. Phys., 13(23), 11925–11933, doi:10.5194/acp-13-11925-2013, 2013.

Shupe, M.: Clouds at Arctic atmospheric observatories: Part II. Thermodynamic phase characteristics, J. Appl. Meteorol. Clim., 50, 645-661, doi:10.1175/2010JAMC2468.1., 2011.

Shupe, M.D., Daniel, J.S., de Boer, G., Eloranta, E.W., Kollias, P., Luke, E., Long, C.N., Turner, D.D., and Verlinde, J.: A focus on mixed-phase clouds: The status of ground-based observational methods, B. Am. Meteorol. Soc., 87, 1549-1562, doi:10.1175/2008BAMS2378.1., 2008.

Earth Syst. Sci. Data Discuss., doi:10.5194/essd-2015-40, 2016
Manuscript under review for journal Earth Syst. Sci. Data
Published: 18 January 2016

Shupe, M.D., Walden, V.P., Eloranta, E., Uttal, T., Campbell, J.R., Starkweather, S.M., and Shiobara, M.: Clouds at Arctic atmospheric observatories. Part I. Occurrence and macrophysical properties, J. Appl. Meteorol. Clim., 50, 626-644, doi:10.1175/2010JAMC2567.1., 2011.

Stamnes, K., Tsay, S.-C., Wiscombe, W. J., and Jayaweera, K.: Numerically stable algorithm for discrete-ordinate-method radiative transfer in multiple scattering and emitting layered media, Appl. Optics, 27(12), 2502–2509, doi:10.1364/AO.27.002502, 1988.

Stamnes, K., Tsay, S.-C., Wiscombe, W., and Laszlo, I.: DISORT, a general-purpose Fortran program for discrete-ordinate-method radiative transfer in scattering and emitting layered media: Documentation of methodology, Tech. rep., Dept. of Physics and Engineering Physics, Stevens Institute of Technology, Hoboken, NJ 07030, 2000.

Stamnes, K., Ellingson, R.G., Curry, J.A., Walsh, J.E., and Zak, B.D.: Review of science issues, deployment strategy, and status for the ARM North Slope of Alaska – Adjacent Arctic Ocean climate research site, J. Climate, 12, 46-63, doi:10.1175/1520-0442-12.1.46, 1999.

Strabala, K.I., Ackerman, S.A., and Menzel, W.P.: Cloud properties inferred from 8-12-μm data, J. Appl. Meteorol., 33, 212-229, 1994.

Turner, D.D.: Arctic mixed-phase cloud properties from AERI lidar observations: Algorithm and results from SHEBA, J. Appl. Meteorol., 44, 427-444, doi:10.1175/JAMC2208.1., 2005.

Turner, D.D., Ackerman, S.A., Baum, B.A., Revercomb, H.E., and Yang, P.: Cloud phase determination using ground-based AERI observations at SHEBA, J. Appl. Meteorol., 42, 701-715, doi:10.1175/1520-0450(2003)042<0701:CPDUGA>2.0.CO;2, 2003.

Uttal, T., Curry, J.A., Mcphee, M.G., Perovich, D.K., Moritz, R.E., Maslanik, J.A., Guest, P.S., Stern, H.L., Moore, J.A., Turenne, R., Heiberg, A., Serreze, M.C., Wylie, D.P., Persson, O.G., Paulson, C.A., Halle, C., Morison, J.H., Wheeler, P.A., Makshtas, A., Welch, H., Shupe, M.D., Intrieri, J.M., Stamnes, K., Lindsey, R.W., Pinkel, R., Pegau, W.S., Stanton, T.P., and Grenfeld, T.C.: Surface Heat Budget of the Arctic Ocean, B. Am. Meteorol. Soc., 83, 255-275, doi:10.1175/1520-0477(2002)083<0255:SHBOTA>2.3.CO;2, 2002.

Earth Syst. Sci. Data Discuss., doi:10.5194/essd-2015-40, 2016
Manuscript under review for journal Earth Syst. Sci. Data
Published: 18 January 2016

Vavrus, S., Waliser, D., Schweiger, A., and Francis, J.: Simulations of 20th and 21st century Arctic cloud amount in the global climate models assessed in the IPCC AR4, Clim. Dyn., 33, 1099-1115, doi: 10.1007/s00382-008-0475-6, 2009.

Vogelmann, A.M, McFarquhar G.M., Ogren, J.A., Turner, D.D., Comstock, J.M., Feingold, G., Long, C.N., Jonsson, H.H., Bucholtz, A., Collins, D.R., Diskin, G.S., Gerber, H., Lawson, R.P., Woods, R.K., Andrews, E., Yang, H.-J., Chiu, J.C., Hartsock, D., Hubbe, J.M., Lo, C., Marshak, A., Monroe, J.W., McFarlane, S.A., Schmid, B., Tomlinson, J.M., and Toto, T.: RACORO extended-term aircraft observations of boundary layer clouds, B. Am. Meteorol. Soc., 93, 861–878, doi:10.1175/BAMS-D-11-00189.1, 2012.

Vömel, H., Selkirk, H., Miloshevich, L., Valvarde-Canossa, J., Vadés, Kyrö, E., Kivi, R., Stolz, W., Peng, G., and Diaz, J.A.: Radiation dry bias of the Vaisala RS92 humidity sensor, J. Atmos. Ocean Tech., 24, 953–963, doi: 10.1175/JTECH2019.1, 2007.

Wang, X. and Key, J.: Arctic surface, cloud, and radiation properties based on the AVHRR Polar Pathfinder dataset. Part I: Spatial and temporal characteristics, J. Climate, 18, 2558-2574, doi:10.1175/JCLI3438.1., 2005.

Wiscombe, W.J.: Improved Mie scattering algorithms, Appl. Optics, 19(9), 1505-1509, doi:10.1364/AO.19.001505, 1980.

Wiscombe, W.J.: Mie scattering calculations: Advances in technique and fast, vector-speed computer codes, NCAR Technical Note NCAR/TN-140+STR, National Center for Atmospheric Research, Boulder, CO, 1979.

Zhao, C., Xie, S., Klein, S.A., Protat, A., Shupe, M.D., McFarlane, S.A., Comstock, J.M., Delanoë, J., Deng, M., Dunn, M., Hogan, R.J., Huang, D., Jensen, M.P., Mace, G.G., McCoy, R., O'Connor, E.J., Turner, D.D., and Wang, Z.: Toward understanding of differences in current cloud retrievals of ARM ground-based measurements, J. Geophys. Res-Atmos., 117, D10206, doi:10.1029/2011JD016792, 2012.

Earth Syst. Sci. Data Discuss., doi:10.5194/essd-2015-40, 2016
Manuscript under review for journal Earth Syst. Sci. Data
Published: 18 January 2016

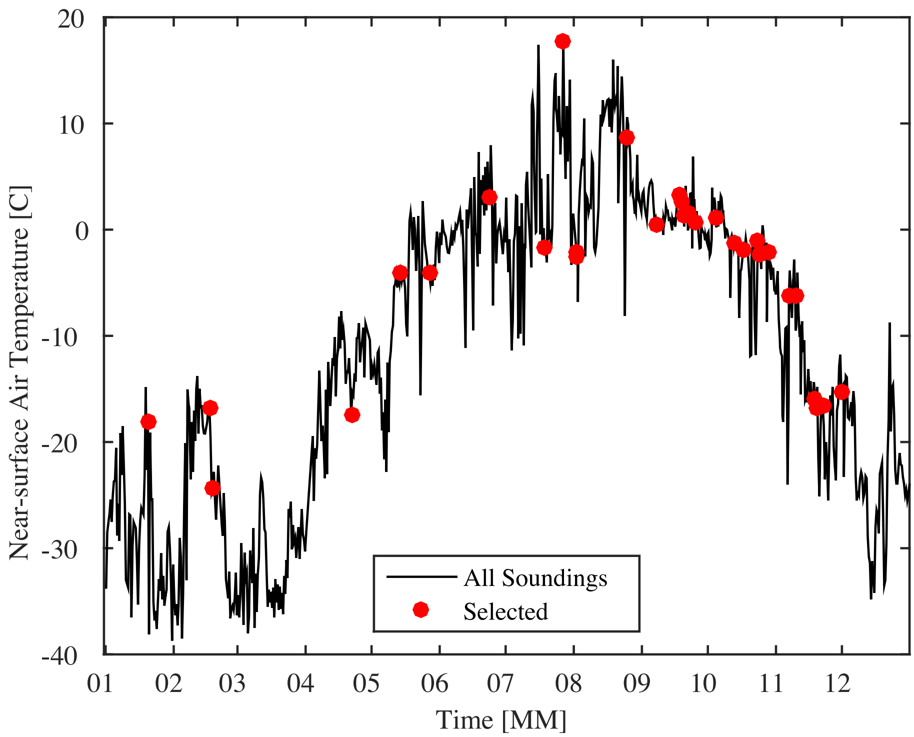

Figure 1. Temperature timeseries for the lowest level of each radiosonde from the 2012 Barrow data set. Red dots represent the 30 radiosondes that were selected for the data set.

Earth Syst. Sci. Data Discuss., doi:10.5194/essd-2015-40, 2016
Manuscript under review for journal Earth Syst. Sci. Data
Published: 18 January 2016

Open Access Earth System Science Data Discussions

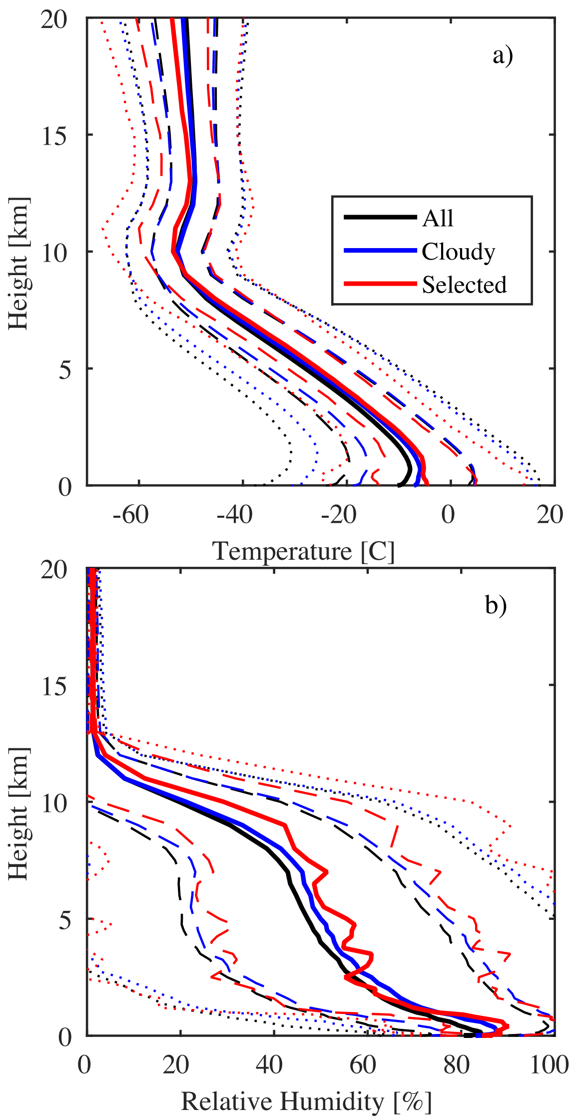

Figure 2. a) Mean profile from 2012 radisondes (black), mean "cloudy" profile (blue), mean of selected radiosondes (red). b) Same as (a), but for relative humidity. Dashed and dotted lines represent +/- 1σ and 2σ variability, respectively

Earth Syst. Sci. Data Discuss., doi:10.5194/essd-2015-40, 2016
Manuscript under review for journal Earth Syst. Sci. Data
Published: 18 January 2016

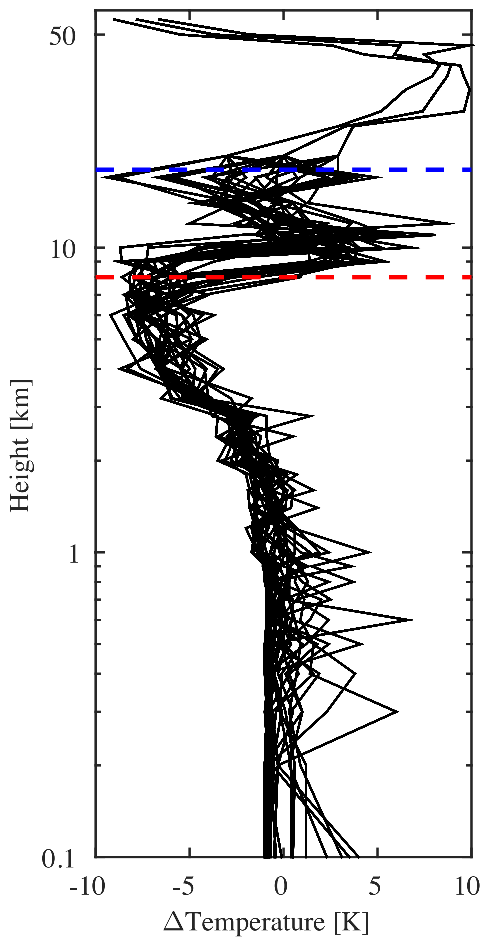

Figure 3. Temperature difference ($T_{layer\ top}$ - $T_{layer\ bottom}$) for each profile. The threshold for the temperature differential was +/- 10 K, which are the limits of the x axis for the plot. The dashed red line is 8km, the highest level that clouds are positioned. The dashed blue line is 18 km; above 18 km only standard atmospheres (sub-Arctic winter, sub-Arctic summer, and the transition seasons) are used. The lines are plotted using the center heights of the layers as the vertical coordinate.

Earth Syst. Sci. Data Discuss., doi:10.5194/essd-2015-40, 2016
Manuscript under review for journal Earth Syst. Sci. Data
Published: 18 January 2016

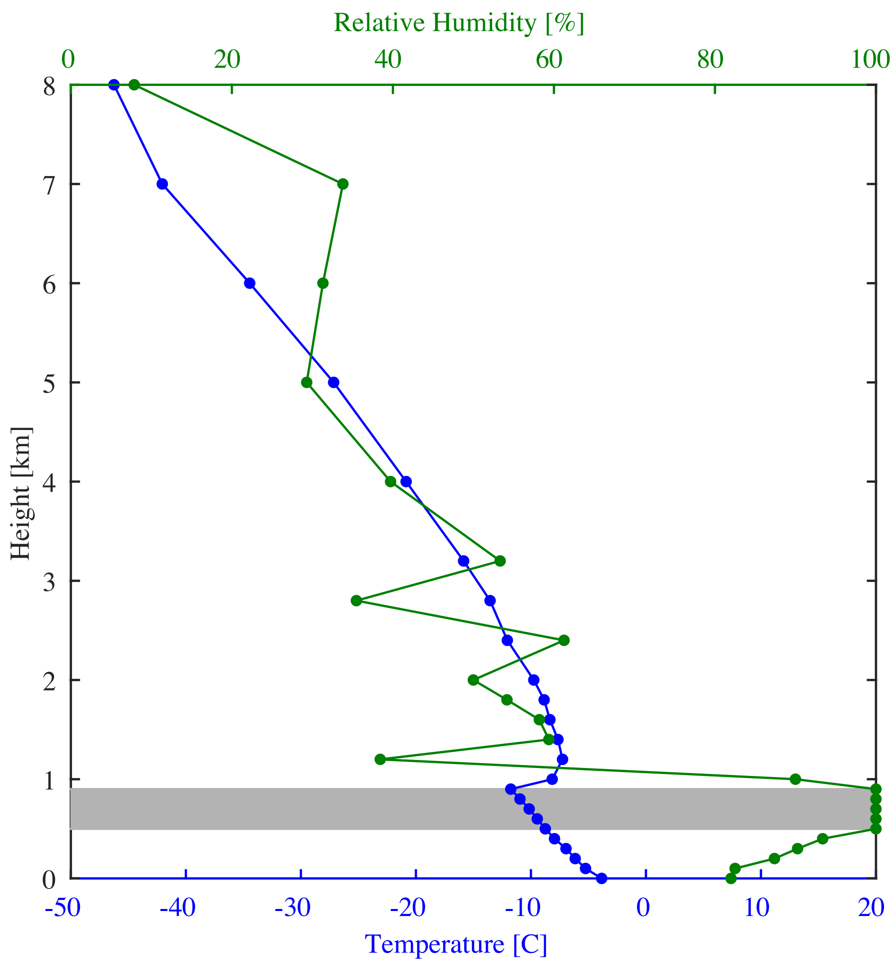

Figure 4. Example profile of temperature (blue) and relative humidity (green) from the surface to 8 km. The cloud (grey shading) is placed between 0.5 an 0.9 km, encompassing 4 model atmospheric layers. The temperature profile exhibits a cloud top inversion.

Earth Syst. Sci. Data Discuss., doi:10.5194/essd-2015-40, 2016
Manuscript under review for journal Earth Syst. Sci. Data
Published: 18 January 2016

Open Access Earth System Science Data Discussions

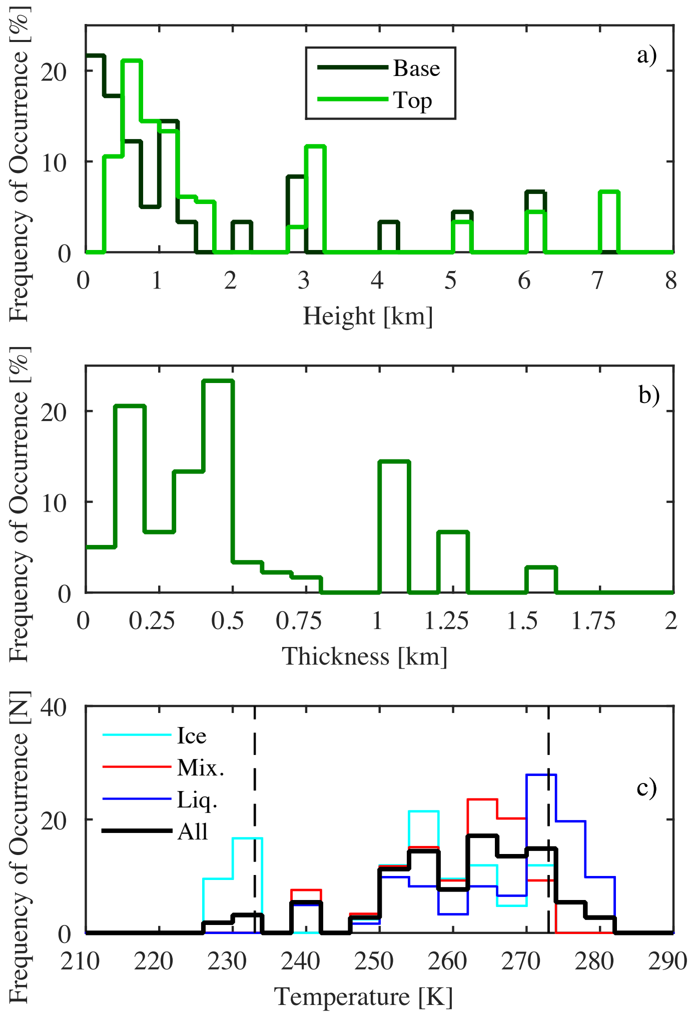

Figure 5. Distributions of macrophysical properties for the 222 simulated clouds. a) cloud base height (black) and cloud top height (gray), b) physical thickness, and c) cloud mean temperature. The vertical lines in (c) represent the physical limits imposed on the minimum temperature that liquid may be included (233 K) and the maximum temperature that ice may be included (273 K). Between these thresholds examples of liquid-only, ice-only, and mixed phase clouds are simulated.

Earth Syst. Sci. Data Discuss., doi:10.5194/essd-2015-40, 2016
Manuscript under review for journal Earth Syst. Sci. Data
Published: 18 January 2016

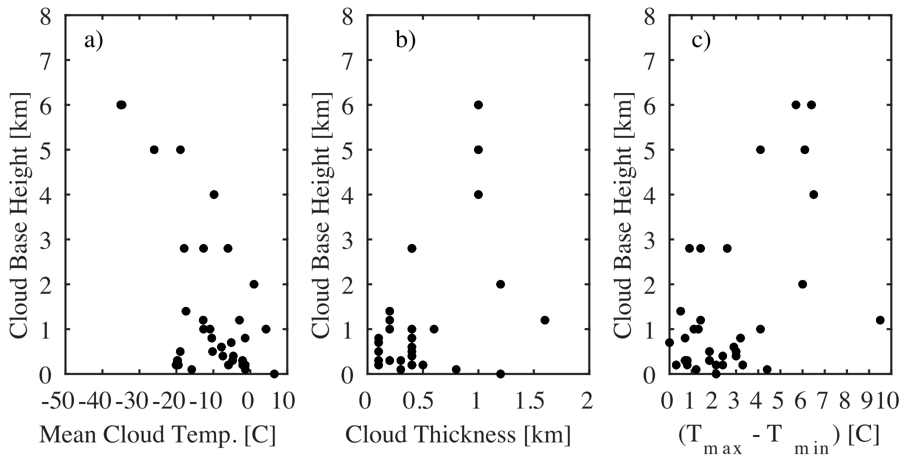

Figure 6. Relationships between the macrophysical properties for the 37 cloud macrophysical scenarios. a) cloud base height versus cloud layer mean temperature, b) cloud base height versus cloud physical thickness, and c) cloud base height versus cloud layer temperature differential.

Earth Syst. Sci. Data Discuss., doi:10.5194/essd-2015-40, 2016
Manuscript under review for journal Earth Syst. Sci. Data
Published: 18 January 2016

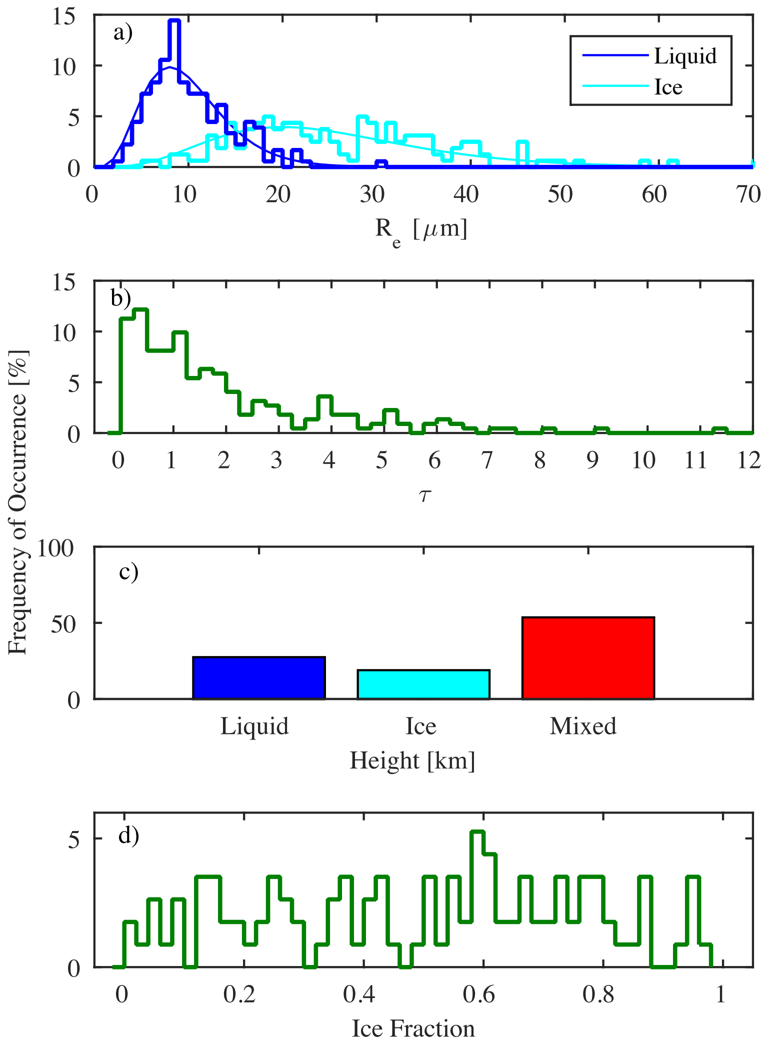

Figure 7. Distributions of microphysical properties for the 222 simulated clouds. a) Effective radius, b) total (ice + liquid) optical depth, c) phase, and d) ice fraction (fraction of total optical depth) for mixed-phase clouds.

Earth Syst. Sci. Data Discuss., doi:10.5194/essd-2015-40, 2016
Manuscript under review for journal Earth Syst. Sci. Data
Published: 18 January 2016

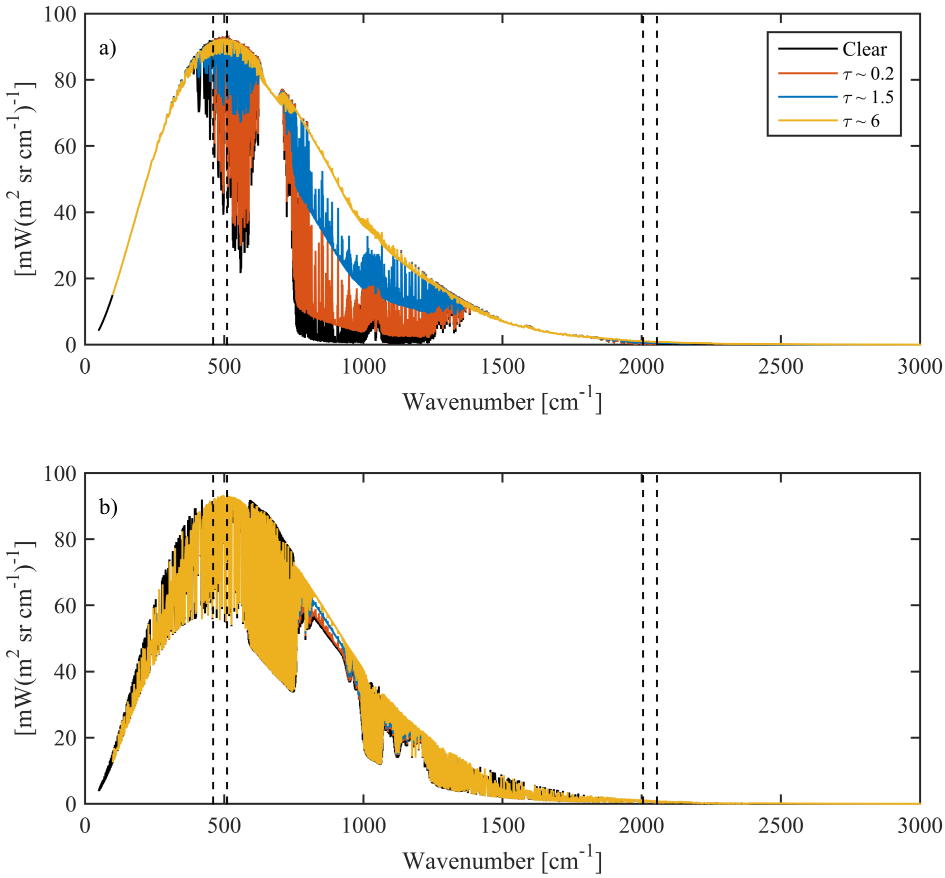

Figure 8. Example simulated radiances for (a) downwelling from the perspective of the surface and (b) same case as (a), but for upwelling radiances from the perspective of the top of atmosphere. Channel edges and channel overlap between ch1 and ch2 are marked by vertical dashed lines near 500 cm^{-1} and similarly near 2000 cm^{-1} for ch2 and ch3. Each panel shows line-by-line clear sky radiances (black) and 0.01 cm^{-1} resolution spectra for three example clouds with optical depths of approximately 0.2 (red), 1.5 (blue), and 6 (yellow).

Earth Syst. Sci. Data Discuss., doi:10.5194/essd-2015-40, 2016
Manuscript under review for journal Earth Syst. Sci. Data
Published: 18 January 2016

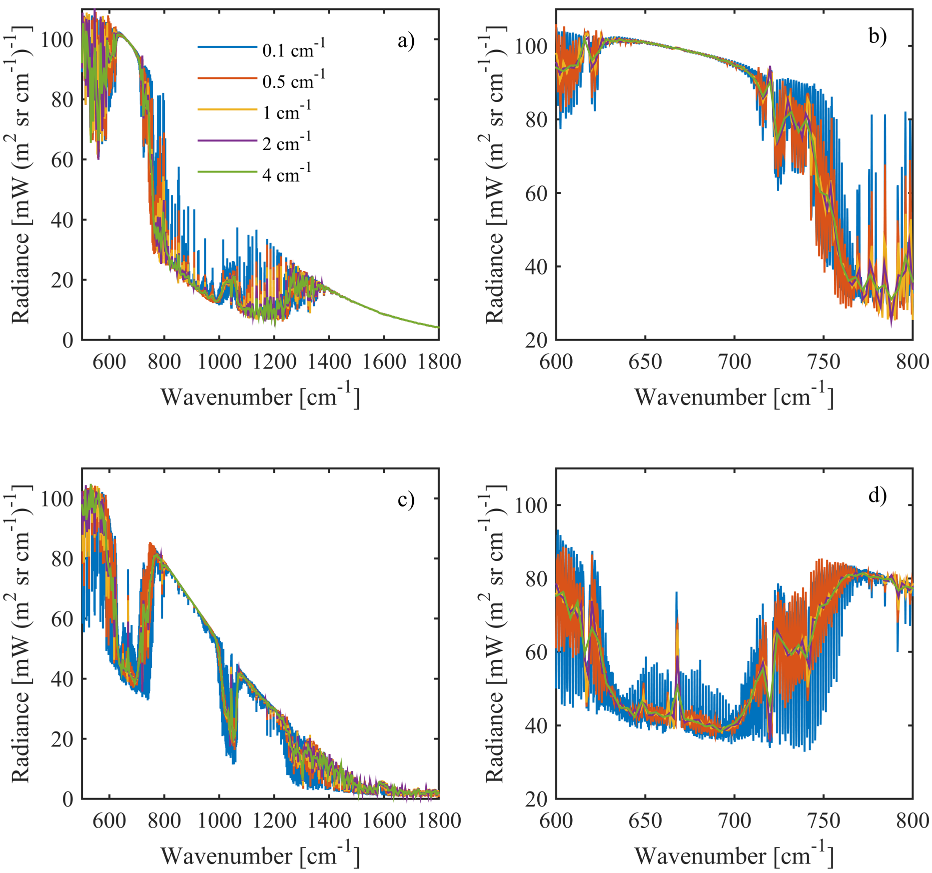

Figure 9. Simulated downwelling radiances from 500-1800 cm^{-1} for an example case (τ = 0.65) from the perspective of the surface (a,b) and simulated upwelling radiances from same case from the perspective of the top of atmosphere (c,d). The top row (a,c) and the bottom row (c,d) each show the same data, but with the x-axis narrowed to 600-800 cm^{-1} to illustrate the wing of the 15 µm CO_2 band where there is considerable spectral structure. In each panel the 0.01 cm^{-1} spectral resolution base data is convolved to 0.1 cm^{-1} (blue), 0.5 cm^{-1} (red), 1 cm^{-1} (yellow), 2 cm^{-1} (purple), and 4 cm^{-1} (green).